Research Article

Received: 20 June 2014 Revised: 26 December 2014 Accepted article published: 11 March 2015 Published online in Wiley Online Library: 10 April 2015

(wileyonlinelibrary.com) DOI 10.1002/ps.4003

Using satellite multispectral imagery for damage mapping of armyworm (*Spodoptera frugiperda*) in maize at a regional scale

Jingcheng Zhang,[a,b,c,d] Yanbo Huang,[e] Lin Yuan,[a,b,c,d] Guijun Yang,[a,b,c,,d] Liping Chen[a,b,c,d] and Chunjiang Zhao[a,b,c,d*]

Abstract

BACKGROUND: Armyworm, a destructive insect for maize, has caused a wide range of damage in both China and the United States in recent years. To obtain the spatial distribution of the damage area, and to assess the damage severity, a fast and accurate loss assessment method is of great importance for effective administration. The objectives of this study were to determine suitable spectral features for armyworm detection and to develop a mapping method at a regional scale on the basis of satellite remote sensing image data.

RESULTS: Armyworm infestation can cause a significant change in the plant's leaf area index, which serves as a basis for infestation monitoring. Among the number of vegetation indices that were examined for their sensitivity to insect damage, the modified soil-adjusted vegetation index was identified as the optimal vegetation index for detecting armyworm. A univariate model relying on two-date satellite images significantly outperformed a multivariate model, with the overall accuracy increased from 0.50 to 0.79.

CONCLUSION: A mapping method for monitoring armyworm infestation at a regional scale has been developed, based on a univariate model and two-date multispectral satellite images. The successful application of this method in a typical armyworm outbreak event in Tangshan, Hebei Province, China, demonstrated the feasibility of the method and its promising potential for implementation in practice.

Keywords: maize; armyworm; multispectral remote sensing; mapping; modified soil-adjusted vegetation index

1 INTRODUCTION

Currently, to prevent damage by pests such as insects, weeds and plant pathogens to crops, a large amount of pesticide is applied worldwide each year. However, the loss of crops because of insects has still increased significantly during the last 50 years.[1,2] The armyworm (*Spodoptera frugiperda*) is an occasional insect that endangers maize crops in summer in northern China. The armyworm is the caterpillar life stage of a moth, which is regarded as a pest to maize. As its name suggests, the armyworm tends to infest maize plants in one field until the crops are exhausted. Then, the entire 'army' will move to another field to feed. In the event of an armyworm outbreak, their feeding habit will wreak havoc in a large area of maize fields, which may result in a huge yield loss. In the autumn of 2012, a nationwide prevalence of armyworm was reported in both China and the United States. In the United States, armyworm spread greatly in Illinois, Tennessee, Kentucky and Montana and caused extensive damage (USDA 26th Congressional District). Meanwhile, in the northern and eastern plains of China, which are major maize-growing regions, severe armyworm infestation was reported at about the same time as in the United States.

Given the rapid development and spread of armyworm, an accurate and rapid assessment of the extent and severity of damage caused by armyworm is of great importance for decision-making in crop production. For example, such information can help the agricultural administration determine whether to implement price regulation or to provide financial subsidies in damaged regions. Moreover, spatial distribution information of insect damage is also vital to agricultural insurance companies.[3] In the event of the 2012 armyworm infestation in China, on account of the lack of an efficient way to conduct field surveys over a large area, the number

* *Correspondence to: Chunjiang Zhao, Beijing Research Centre for Information Technology in Agriculture, Beijing 100097, China. E-mail: zhaochjrs@126.com*

a *Beijing Research Centre for Information Technology in Agriculture, Beijing, China*

b *National Engineering Research Centre for Information Technology in Agriculture, Beijing, China*

c *Key Laboratory for Information Technologies in Agriculture, the Ministry of Agriculture, China*

d *Beijing Engineering Research Center of Agricultural Internet of Things, Beijing, China*

e *USDA-ARS, CPSRU, 141 Experiment Station Road, Stoneville, MS 38776, USA*

of investigators available to insurance companies to carry out the necessary surveys was insufficient, which resulted in many financial disputes.

In recent years, remote sensing technology has been developed extensively. This development has made possible spatial-temporal field observation over a large area. Spatially continuous information from observations enables precision crop management (PCM), which involves variable-rate applications for fertilisation and fungicide spraying.[4,5] It is known that plants under stress will exhibit specific symptoms (e.g. reduction in the leaf area index, destruction of pigments, variation in canopy morphology), which can be manifested by certain responses in the plant leaf visible/near-infrared (VIS-NIR) spectrum.[6–9] Based on spectral measurements made at the leaf and canopy levels, a number of spectral features (i.e. various vegetation indices and other forms of feature) were developed/examined for detecting crop stresses.[7,8] Liu *et al.*[10] identified the red-edge (680–740 nm spectral region) width as an indicator of water stress for wheat plant. Through examination and comparison with several classic vegetation indices for detecting the plant's nitrogen and chlorophyll content, Chen *et al.*[11] proposed a novel index called the double-peak canopy nitrogen index, which is more sensitive to nitrogen deficiency in plants. For plant pests and diseases, a number of studies have been conducted that have resulted in a set of vegetation indices (e.g. the normalised difference vegetation index, the photochemical reflectance index, the anthocyanin reflectance index) for detecting yellow rust, powdery mildew, aphid in wheat,[12–15] late blight in tomato, leaf blight disease, brown planthopper and leaffolder in rice,[16–19] spider mite in cotton and several other types of disease/pest.[8,20,21] In addition, based on the identified spectral features, the capability of airborne and satellite remote sensing images in mapping diseases/pests has been evaluated. Huang *et al.*[22] used hyperspectral airborne images for mapping yellow rust in winter wheat.[22] In their study, a satisfactory accuracy was reached ($R^2 = 0.91$). Apart from hyperspectral imagery, the potential of multispectral imagery in mapping crop diseases/pests was also evident. Qin and Zhang[23] applied an airborne multispectral image to map the damage caused by rice sheath blight. A reasonable correlation coefficient (0.62) between image-based vegetation indices and disease severity suggested that the spatial trend of disease severity could be generated by multispectral remote sensing. Franke and Menz[24] successfully monitored leaf rust and powdery mildew in winter wheat with a high-resolution satellite image (Quickbird). In mapping cotton root rot, Yang[19] compared the performance of multispectral and hyperspectral images. The results suggested that both forms of data produced approximately equal mapping accuracy, which thus encouraged multispectral-data-based applications with a lower cost and a higher availability.[19] As an example for such application cases, Chen *et al.*[25] successfully detected take-all disease in winter wheat with a moderate-resolution satellite multispectral image (Landsat 5 TM).

Research progress and practical applications of remote sensing in agriculture, as reviewed above, motivated us to attempt to map the extent and severity of armyworm damage with satellite multispectral data. Given the fact that armyworm infestation usually occurs at a relatively large spatial scale, images acquired by the environment and disaster reduction small satellite (HJ-CCD), a satellite remote sensing system launched by China in 2008 for land resource observation, were used in this study. The data have a 30 m spatial resolution with four bands in blue, green, red and NIR, a broad imaging swath (360 km) and a short revisit frequency (<4 days) (Table 1). In the summer of 2012, a serious armyworm outbreak provided a good opportunity to examine the capability of HJ-CCD images in mapping the insect damage. The objectives of this study were (1) to identify suitable spectral features specifically for detecting armyworm infestation, (2) to develop a mapping method at a regional scale for monitoring the spatial distribution of armyworm using two-date satellite remote sensing image data and (3) to assess the performance of the developed method with comprehensive ground survey data.

Table 1. Parameters and information of HJCCD images

Category	Items	Information	
Parameters of sensors	Sensor	CCD	
	Platform	HJ-1A/B satellites	
	Spatial resolution (m)	30	
	Spectral range (nm):		
	Band 1	430–520	
	Band 2	520–600	
	Band 3	630–690	
	Band 4	760–900	
	Image swath (km)	360	
	Revisit time (days)	4	
Acquisition information of scenes	Date	16 July	13 August
	Scene ID	832675	853839
	Path (P) and row (R)	454/68	454/68

2 METHODS

2.1 Study area and the armyworm attack event

A site suffering an attack of armyworms in the summer of 2012 was selected as the study area for this study. The site, with a total area of over 3000 km^2, was located in the northern part of the North China Plain (39.75° N, 118.19° E), characterised by flat terrain (average elevation around 40 m). The study area was composed of three regions: Tangshan City, Fengrun County and Luan County (Fig. 1). In the study area, maize is a major crop that is planted in summer from late June to late September in a year. Armyworm outbreaks are always related to weather conditions and the generation time of the pest. However, given that the emergence timing of moths and the timing of favourable weather conditions for armyworm are highly variable, it is very challenging to forecast an outbreak precisely. In the summer of 2012, a significant rainfall event was coincident with the emergence of third-instar larvae of armyworm in several places in northern China, which thus led to a severe outbreak of armyworm across the maize-planted areas in northern China. According to weather records made from a total of 14 weather stations around the study area, over 220 mm of continuous rain fell from 21 July to 5 August 2012 (Fig. 2), which thus formed favourable weather conditions for armyworm (i.e. cool and wet conditions). With a significant increase in the number of eggs laid by the second-generation moth, a severe armyworm infestation occurred on 6–10 August, according to records from the local Plant Protection Agency.

2.2 Field investigation

In this study area, a total of 69 plots were randomly selected and surveyed for damage severity of armyworm in August 2012, with 41 plots for model calibration and the remaining 28 plots for validation (Fig. 1). The sampling design was according to the

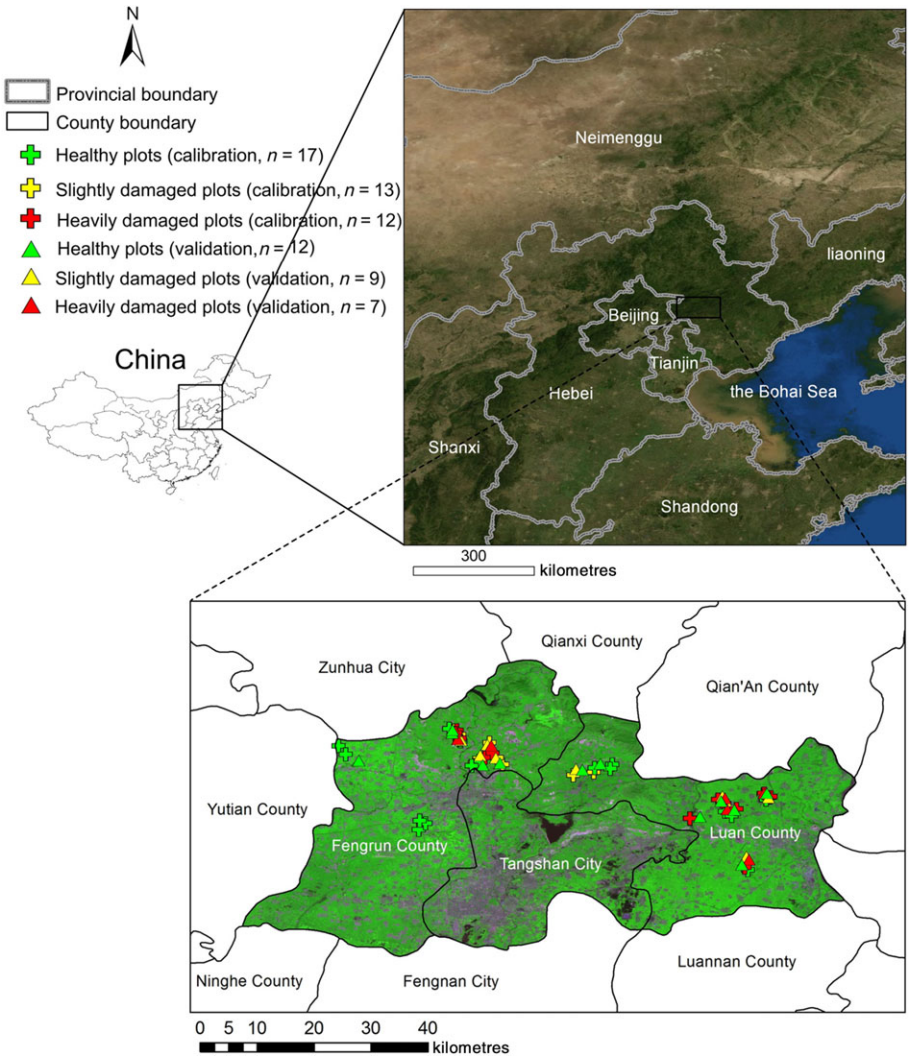

Figure 1. A map of survey points in the study area in Hebei Province, China.

North America Weed Management Association (NAWMA) mapping standard.[26] To relate the plots to corresponding image pixels, a continuous maize planting area covering a circle of 20 m radius was investigated. Within each plot, three transects from the plot's central point to its perimeter at 30° N, 150° N and 270° N were surveyed (Fig. 3). Along each transect, a total of 20 maize plants were randomly selected for inspection. To assess the infestation status and damage severity for each plot, a semi-quantitative method was applied in the study. Each plot needed to be assigned to one of three severity classes, including healthy, slightly damaged and severely damaged. The healthy class indicated that the plot had not been infested or that total leaf damage had occurred on less than 5% of the surveyed plants. For damaged plots, as the three-ear leaves are of significant importance to the photosynthesis of maize plants,[27] the outcome caused by armyworm was mainly dependent on whether the three-ear leaves had been damaged. Therefore, the slightly damaged class was defined as less than 30% damage to three-ear leaves, and the severely damaged class as over 30% damage to three-ear leaves (Fig. 4).[28]

Among the biophysical parameters, the most significant damage by armyworms is to cause a reduction in leaf area index (LAI) and biomass.[29] Moreover, the chlorophyll content (Chl) was also reported to have a certain correlation with insect damage.[30] Within our surveyed plots, 27 plots were selected to measure both LAI and Chl. LAI measurements per transect were made using a LAI-2000 plant canopy analyser (LI-COR, Lincoln, NE) in three 1×1 m subplots, with ten repeats. For Chl measurement, a SPAD chlorophyll meter (Konika Minolta, Osaka, Japan) was used to measure three-ear leaves. In each subplot, three maize plants were randomly measured, with five repeats. All measurements for both parameters were firstly averaged at a subplot level and then averaged to represent the entire plot.

2.3 HJ-CCD data and preprocessing

For this study, two cloud-free HJ-CCD scenes were acquired before (16 July) and after (13 August) the outbreak of armyworm in the study area. The HJ-CCD images were preprocessed with radiometric calibration, atmospheric correction and geometric correction. The calibration coefficients of HJ-CCD were acquired from the China Centre for Resources Satellite Data and Application (CRESDA) in Beijing, China. The calibrated data were then processed for atmospheric correction with the algorithm provided by Liang *et al.*[31], which was used to estimate the spatial distribution of atmospheric aerosols and retrieved surface reflectance under general atmospheric and surface conditions. The original HJ-CCD

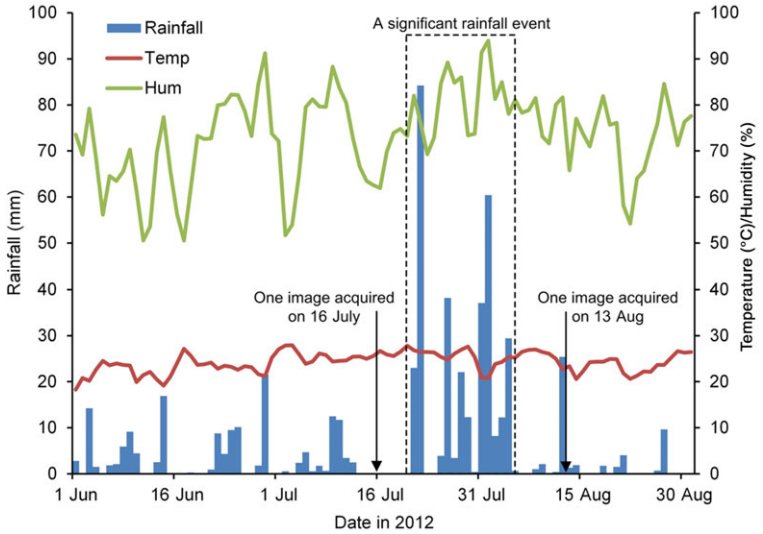

Figure 2. Temporal dynamics of meteorological factors during July and August 2012.

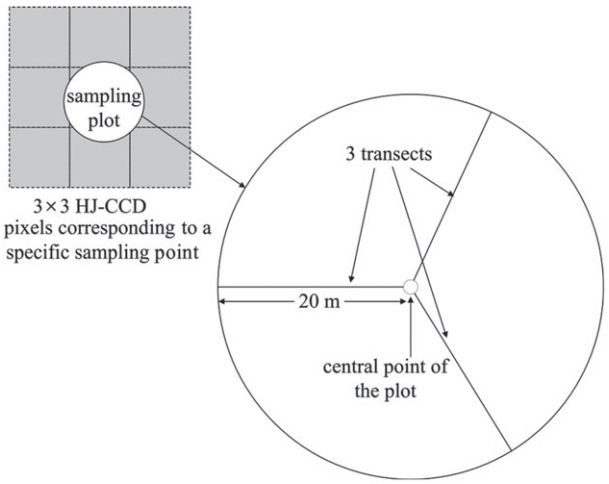

Figure 3. A demonstration of the field sampling method.

images had a systematic geometric correction only. To facilitate change detection analysis, both images on different dates were coregistrated against a historical Landsat ETM+ image with precise geometric correction. According to over 80 ground tie-points selected for the geometric correction, the resulting root mean square error for both images was less than 0.5 pixels.

In the study area, apart from maize, rice and peanuts were planted synchronously. Given that the spectral divergences among different crops are always greater than those between healthy and insect-infested areas inside a crop field, prior to mapping the armyworm, a supervised classification was implemented to produce a mask layer of maize.[32] As the visual difference among maize, rice and peanut could be clearly observed on the HJ-CCD image acquired on 13 August, this image was used directly to execute the classification. Firstly, the vegetated area was differentiated from the non-vegetated area through a simple threshold of the NIR band. Within the vegetated area, maize was the main crop, which was planted together with a small portion of rice, beans and some vegetables. To extract the maize area, a total of 102 points were visually identified from the HJ-CCD image as a reference. With a maximum likelihood classifier (MLC), an overall accuracy of 92% classification was achieved, which can satisfy the accuracy requirement of subsequent damage mapping for infestation analysis (Fig. 5).

2.4 Mapping armyworm-infested areas

A workflow of mapping armyworm-infested areas is displayed in Fig. 6. Firstly, the HJ-CCD images that were acquired before and after the armyworm infestation event were preprocessed by radiometric calibration and atmospheric and geometric corrections to obtain the corresponding surface reflectance images. Then, with an analysis of variance (ANOVA) to examine the sensitivities of several candidate spectral features, a set of optimal spectral features for insect damage mapping were selected. Within the maize area extracted by supervised classification, the maize damage caused by armyworm infestation was mapped using two strategies: a stepwise threshold optimisation based on a single spectral feature, and a maximum likelihood classification based on multiple spectral features. The mapping accuracies by the two methods were assessed and compared on the basis of field investigation data collected in 2012.

2.4.1 Spectral features for mapping armyworm damage

Considering the possible biological impact of armyworm infestation, four classic vegetation indices (VIs) related to LAI, Chl and canopy morphology variations were selected for mapping the damage: the normalised difference vegetation index (NDVI); the soil-adjusted vegetation index (SAVI); the triangular vegetation Index (TVI); the renormalised difference vegetation index (RDVI). Among them, the NDVI is the best-known and most widely used VI for mapping the amount of green biomass in vegetation of low to moderate density.[33] The RDVI modifies the NDVI to make the index more suitable for low to high LAI values.[34] The TVI accounts for radiant energy absorption of chlorophyll,[35] whereas the SAVI is used to minimise soil influences on canopy spectra, which is suitable for observing severely damaged fields with different proportions of soil exposure.[34] In addition, it is worth noting that Haboudane *et al.*[36] made important modifications to TVI and SAVI, resulting in two important new indices: modified SAVI (MSAVI) and modified TVI (MTVI). The general idea behind these modifications was to render the indices less sensitive to chlorophyll effects, more

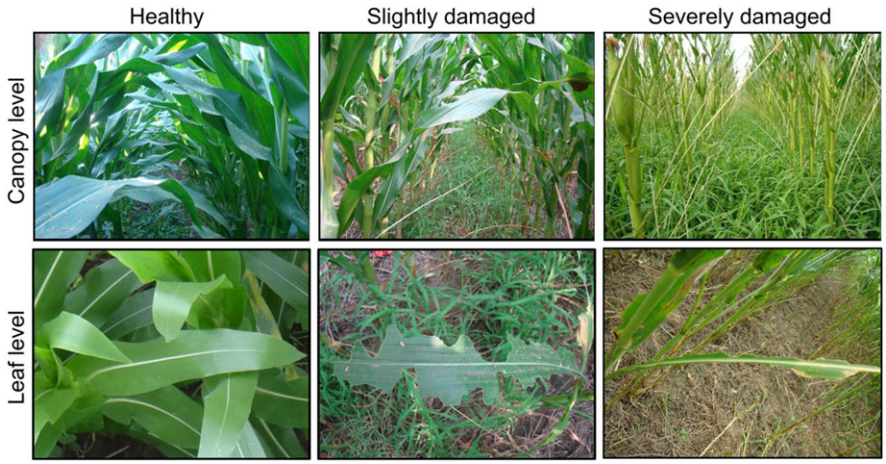

Figure 4. Demonstration of damaged maize due to armyworm at leaf and canopy levels.

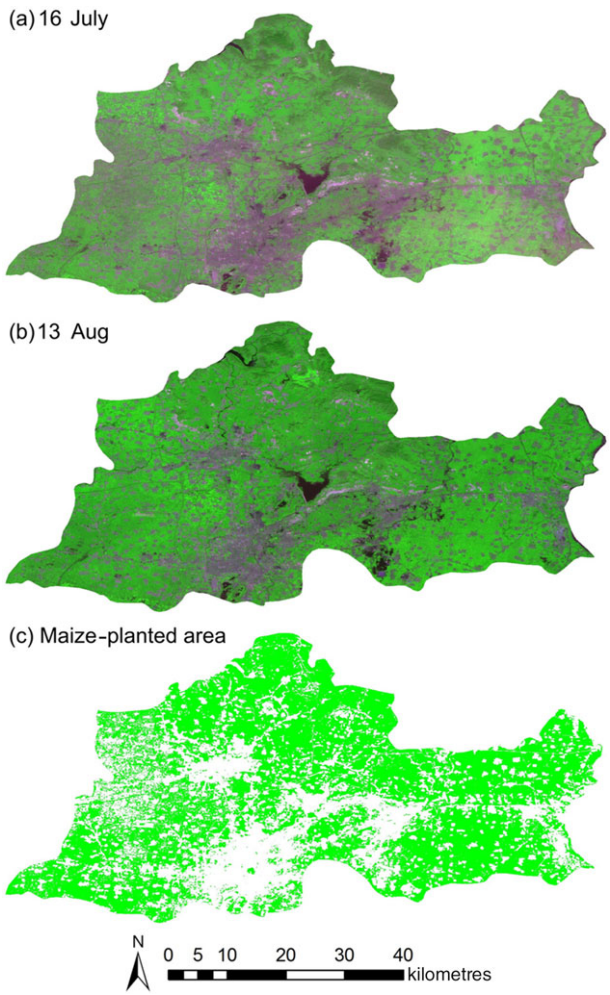

Figure 5. Two-date HJCCD images and maize-planted area.

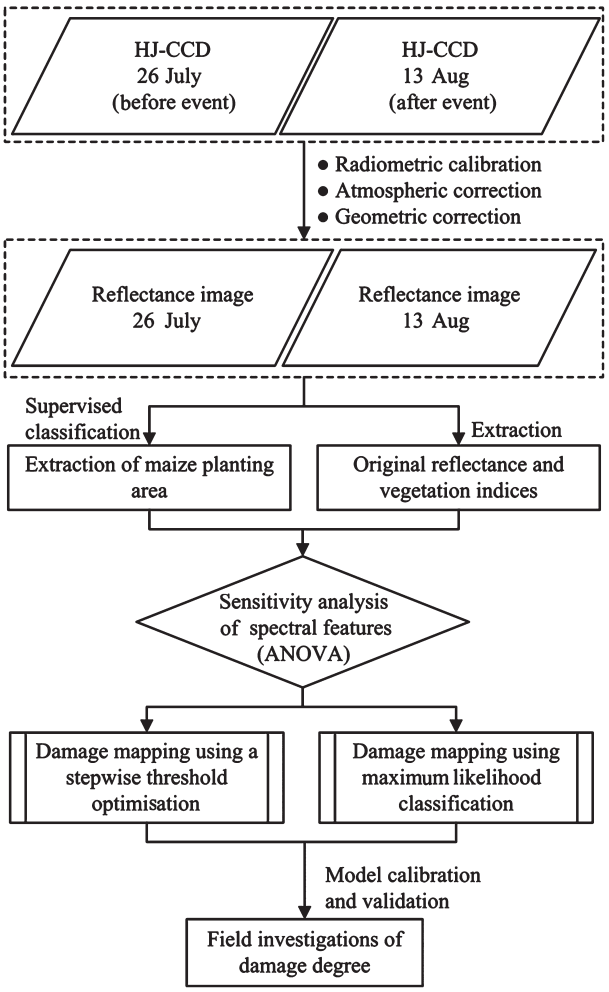

Figure 6. A workflow of armyworm damage mapping at a regional scale.

responsive to green LAI variations and more resistant to soil and atmosphere effects. To conduct a systematic evaluation of spectral features (band reflectance and VIs) for damage mapping, the four original HJ-CCD bands (i.e. blue, green, red and NIR bands) plus all six VIs described above were included. The characteristics, formulas and references[33–38] of all the VIs are given in Table 2.

For these spectral features (SFs), we calculated the change in magnitude from the 16 July image to the 13 August image by using normalisation quantification, which can be written as[39]

$$SF_{change} = \frac{SF_{13\ Aug} - SF_{16\ Jul}}{SF_{13\ Aug} + SF_{16\ Jul}} \quad (1)$$

Table 2. A list of vegetation indices selected for this study

Vegetation index	Formula	Literature
NDVI	$(R_{NIR} - R_R)/(R_{NIR} + R_R)$	Rouse *et al.*[33]
SAVI	$(1 + L)*(R_{NIR} - R_R)/(R_{NIR} + R_R + L)$; $L = 0.5$	Huete[37]
TVI	$0.5*[120*(R_{NIR} - R_G) - 200*(R_R - R_G)]$	Broge and Leblanc[35]
RDVI	$(R_{NIR} - R_R)/(R_{NIR} + R_R)^{0.5}$	Reujean and Breon[34]
MSAVI	$0.5*\{2R_{NIR} + 1 - [(2R_{NIR} + 1)^2 - 8*(R_{NIR} - R_R)]^{0.5}\}$	Qi *et al.*[38]
MTVI	$\frac{1.5[1.2(R_{NIR}-R_G)-2.5(R_R-R_G)]}{\sqrt{(2R_{NIR}+1)^2-(6R_{NIR}-5\sqrt{R_R})-0.5}}$	Haboudane *et al.*[36]

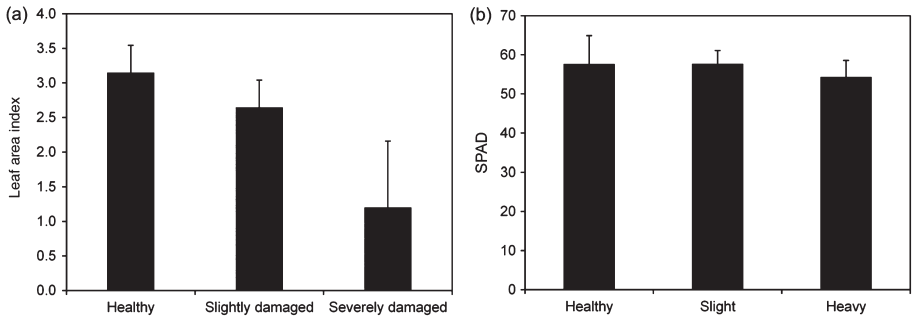

Figure 7. Means and standard deviations of LAI and SPAD (reflecting the Chl content) for healthy and armyworm-infested samples.

where SF_{change} is the two-date SF change, and $SF_{13\ Aug}$ and $SF_{16\ July}$ are the SFs extracted from the images acquired before and after the insect attack respectively.

2.4.2 Analysis of the sensitivity of biophysical parameters and SFs to insect damage

To examine whether the measured LAI and Chl are sensitive to insect damage, a standard ANOVA was applied. In addition, the same analysis was also performed on the selected SFs to identify those that were optimal for damage mapping. For significant *F*-values, homogeneous subgroups were identified according to Tukey's test, with a significance level $\alpha = 0.05$. Only SFs achieving significant difference in at least one pair of groups were retained in subsequent analysis.

2.4.3 Insect damage mapping using a stepwise threshold optimisation

To map insect damage with a single variable, stepwise threshold optimisation was adopted for generating the cut-off values, to avoid using a subjective cut. For this purpose, 100 evenly spaced intervals were set within the data range (i.e. from minimum to maximum) for each variable. Using the validation data, the overall accuracy was calculated by traversing all intervals. The cut-off value was defined as the point where the highest accuracy was reached. Such stepwise-optimised thresholding was applied firstly to generate the cut-off value for separating healthy and slightly damaged samples, and then to identify the cut-off value for differentiating between slightly damaged and severely damaged samples. A similar stepwise optimisation protocol demonstrated effectiveness in vegetation-associated image classification applications.[40,41]

2.4.4 Insect damage mapping using maximum likelihood classification

In addition to mapping insect damage with single variables, a multivariate mapping method was also tested. Prior to the mapping process, a cross-correlation check was performed on spectral features that passed the sensitivity test (in Section 2.4.2) to assess the dependency of variables. If any two variables had an R^2 value of over 0.8, then one variable with lower discriminative capability (according to the results of ANOVA) was abandoned, which thus reduced the information redundancy among variables. In consideration of both efficiency and accuracy of classification, a simple and standard algorithm, the maximum likelihood classification (MLC), was used to produce insect damage maps.

2.5 Accuracy assessment

Mapping results were assessed against validation data. A number of accuracy indices were used, including overall accuracy, producer's accuracy, user's accuracy and kappa coefficient.[42]

3 RESULTS

3.1 Response of biophysical parameters and spectral features to armyworm attack

The means and standard deviations of LAI and Chl at varying damage levels according to the field measurement of biophysical parameters are compared in Fig. 7. It was obvious that the LAI tended to decrease with insect damage, whereas the change in chlorophyll content was less significant. The results of ANOVA also supported this observation. It was found that the LAI was significantly different between severely damaged and the other levels, whereas no statistical difference was found in chlorophyll content between any of the classes.

The responses of the four original band reflectances and various VIs to insect damage are illustrated in Fig. 8, where their means and standard deviations at different damage levels are compared. To show whether the temporal changes in spectral features have higher sensitivity to insect infestation than single-date spectral features, the responses of spectral features extracted from the August 2013 image are also included in Fig. 8 for comparison.

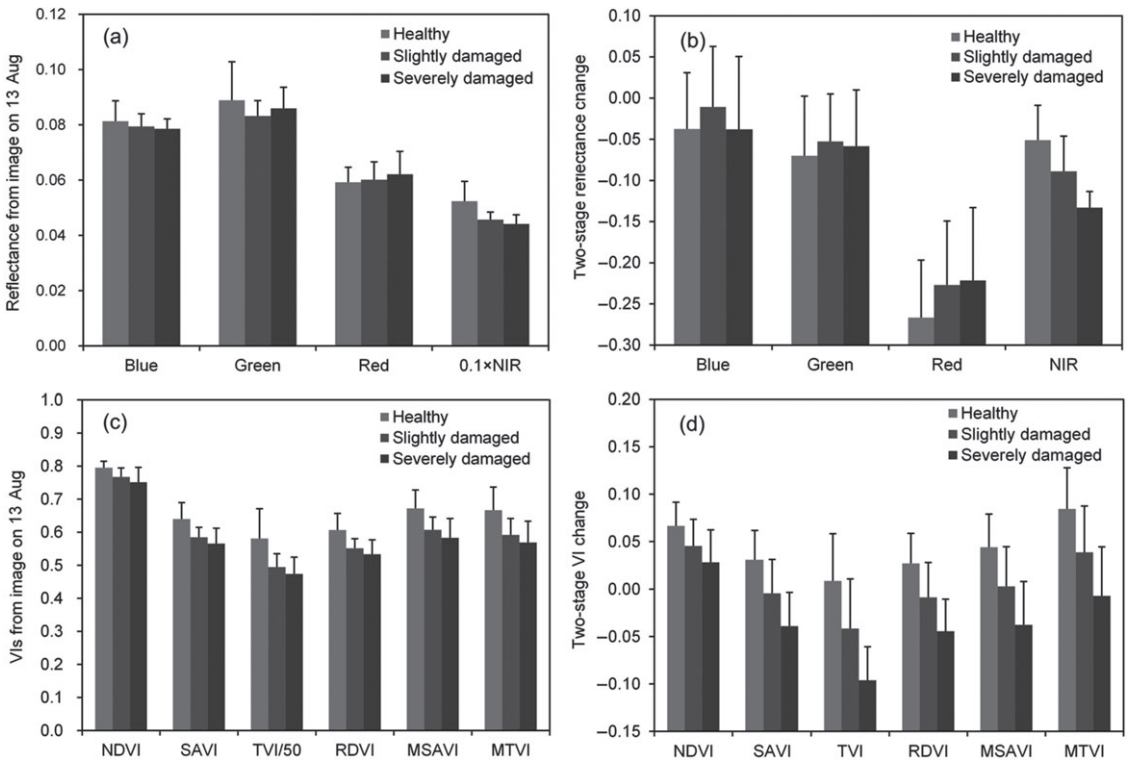

Figure 8. Means and standard deviations of image-based reflectance and VIs.

Table 3. Sensitivity of various imagery-based spectral features[a] based on ANOVA

	Means of two dates			Means on 13 August		
Spectral features	Healthy	Slightly damaged	Severely damaged	Healthy	Slightly damaged	Severely damaged
Blue	−0.0375a	−0.0108a	−0.0378a	0.0813a	0.0794a	0.0786a
Green	−0.0699a	−0.0525a	−0.0583a	0.0889a	0.0832a	0.0859a
Red	−0.2666a	−0.2271a	−0.2214a	0.0592a	0.0601b	0.0621b
NIR	−0.0511a	−0.0890b	−0.1330c	0.0523a	0.0457b	0.0441b
NDVI	0.0666a	0.0454ab	0.0283b	0.7950a	0.7669ab	0.7513b
SAVI	0.0308a	−0.0045b	−0.0391c	0.6399a	0.5847b	0.5655b
TVI	0.0086a	−0.0416b	−0.0961c	0.5806a	0.4946b	0.4737b
RDVI	0.0269a	−0.0087b	−0.0445c	0.6062a	0.5515b	0.5333b
MSAVI	0.0441a	0.0028b	−0.0378c	0.6719a	0.6070b	0.5831b
MTVI	0.0845a	0.0388b	−0.0071c	0.6663a	0.5916b	0.5687b

[a] For each spectral feature, means within a row followed by the same letters are not significantly different according to ANOVA and Tukey's test ($P > 0.05$).

Generally, most band reflectances and VIs showed a certain response to insect damage, except for the reflectance in the green band on 13 August and the two-date reflectances in the blue and green bands. The VIs showed a stronger response than the original band reflectance. Moreover, among the various forms of spectral feature, it should be noted that the two-date VIs exhibited stronger sensitivity to insect damage. The results of ANOVA provided a quantitative measure of the discriminative capability of band reflectances and VIs (Table 3). Among single-date spectral features, eight out of ten features showed significant difference between classes. However, they could only differentiate between healthy and damaged samples and were unable to discriminate levels of insect infestation (i.e. slightly or severely damaged). In contrast, all of the two-date spectral features except NDVI showed significant differences among all groups, which indicated that these spectral features were able not only to differentiate between healthy and damaged samples but also to determine levels of damage severity. To explore the degree of cross-correlation among these spectral features, a correlation matrix summarising the R^2 values between each pair of two-date insect-sensitive spectral features is given in Table. 4. Based on the threshold of $R^2 = 0.8$, only three spectral features – NIR, NDVI and MSAVI – were retained to construct a multivariate model for insect damage mapping.

3.2 Mapping insect damage with two-date satellite imagery

Based on the proposed mapping protocol, damage maps for maize armyworm were produced by each spectral feature using

Table 4. Cross-correlation among insect-sensitive spectral features

R^2	NIR	NDVI	SAVI	TVI	RDVI	MSAVI	MTVI
NIR	1						
NDVI	0.04	1					
SAVI	0.57	0.62	1				
TVI	0.87	0.28	0.87	1			
RDVI	0.62	0.58	0.99	0.90	1		
MSAVI	0.49	0.69	0.99	0.81	0.97	1	
MTVI	0.43	0.71	0.95	0.78	0.93	0.97	1

a univariate model and by their combination using a multivariate model (Figs 9 and 10). These damage maps for different spectral features/combinations showed similar spatial patterns of insect infestation, with relatively serious damage occurring in the north-eastern part and at the southern edge of Fengrun County and in the northern part of Luan County. Such a distribution pattern is generally consistent with the pattern observed in the field. Our field survey showed that insect infestation was heavier in the north-eastern part of Fengrun County and in the northern part of Luan County than in the remaining areas in the region. The damage at the southern edge of Fengrun County was confirmed through telephone interviews with local farmers. To provide a quantifiable result, the accuracies in mapping the armyworm with two-date spectral features are summarised in Tables 5 and 6, as well as the confusion matrices. For individual spectral features, the overall accuracy ranged from 0.64 to 0.79, with MSAVI having the highest accuracy. The multivariate model relying on a combination of spectral features produced an overall accuracy of 0.50, which is lower than the accuracy of all univariate model results. This might suggest that insect damage could be effectively mapped in a simpler and less expensive manner.

To examine whether mapping the insect damage with two-date spectral change information has a significant benefit compared with single-date mapping, the same univariate and multivariate models were calibrated and validated on the basis of single-date features (extracted from the 13 August image), which produced singe-date damage maps for comparison. As shown in Fig. 11, the identified damage area on the single-date damage maps is significantly larger than that on the two-date damage maps. In Tables 6 and Table 7, the large commission errors of the single-date damage mapping results are significantly greater than those of the two-date damage mapping results, which suggests that the insect infestation is seriously overestimated by single-date spectral features or their combination. This issue of the single-date damage mapping protocol resulted in a significant reduction in

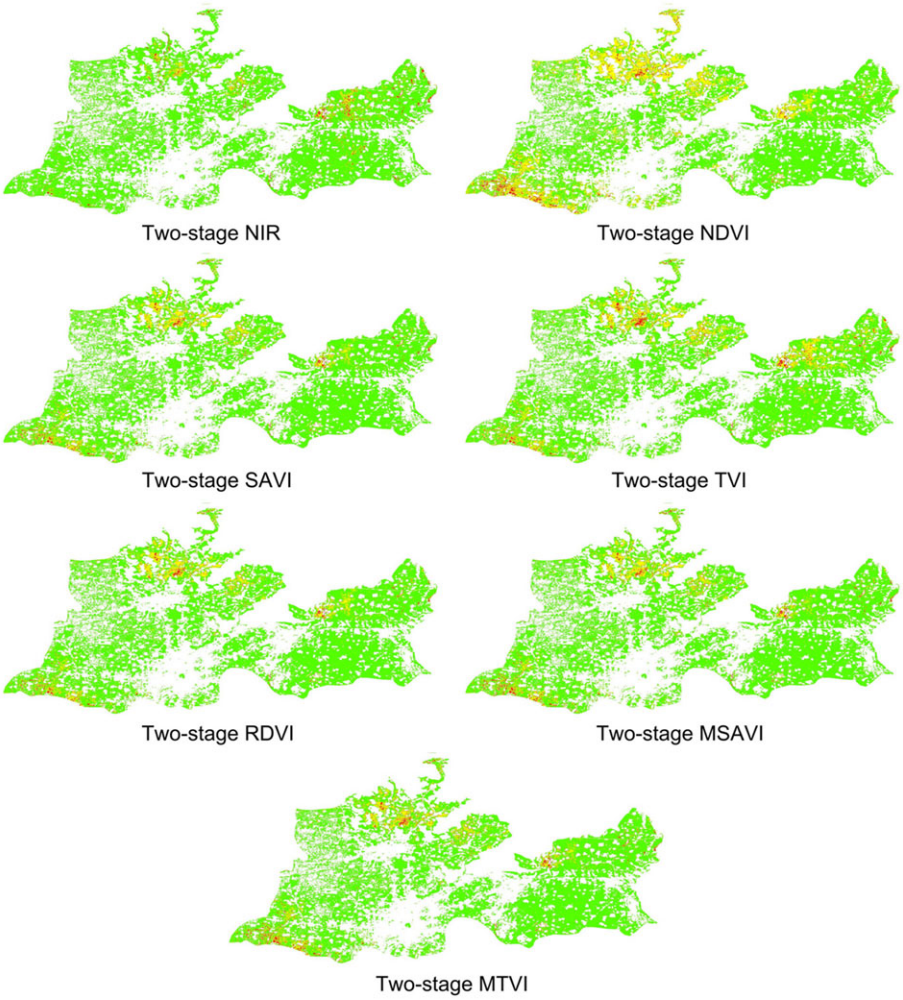

Figure 9. Mapping of armyworm damage based on two-date spectral features.

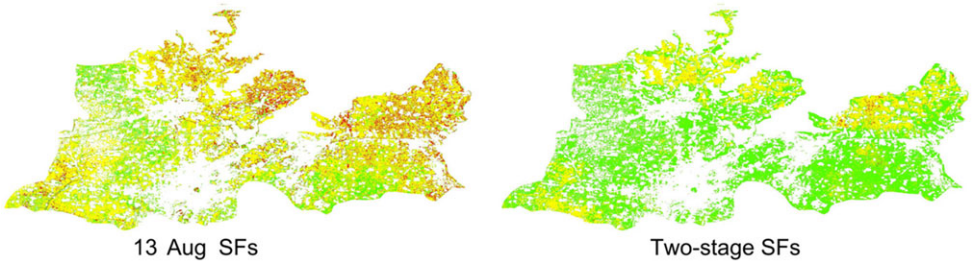

Figure 10. Mapping of armyworm damage based on individual spectral features from a single-date image.

Table 5. Confusion matrices and classification accuracies produced by individual spectral features from two-date images

Predicted classes	Reference				User's accuracy (%)	Overall accuracy (%)	kappa coefficient
	Healthy	Slightly damaged	Severely damaged	Sum			
NIR							
Classed as healthy	9	5	0	14	64.29	0.68	0.50
Classed as slightly damaged	3	4	1	8	50.00		
Classed as severely damaged	0	0	6	6	100.00		
Sum	12	9	7	28			
Producer's accuracy (%)	75.00	44.44	85.71				
NDVI							
Classed as healthy	7	2	0	9	77.78	0.68	0.51
Classed as slightly damaged	5	7	2	14	50.00		
Classed as severely damaged	0	0	5	5	100.00		
Sum	12	9	7	28			
Producer's accuracy (%)	58.33	77.78	71.43				
SAVI							
Classed as healthy	8	2	0	10	80.00	0.71	0.56
Classed as slightly damaged	4	7	2	13	53.85		
Classed as severely damaged	0	0	5	5	100.00		
Sum	12	9	7	28			
Producer's accuracy (%)	66.67	77.78	71.43				
TVI							
Classed as healthy	6	1	0	7	85.71	0.64	0.47
Classed as slightly damaged	5	7	2	14	50.00		
Classed as severely damaged	1	1	5	7	71.43		
Sum	12	9	7	28			
Producer's accuracy (%)	50.00	77.78	71.43				
RDVI							
Classed as healthy	8	2	0	10	80.00	0.71	0.56
Classed as slightly damaged	4	7	2	13	53.85		
Classed as severely damaged	0	0	5	5	100.00		
Sum	12	9	7	28			
Producer's accuracy (%)	66.67	77.78	71.43				
MSAVI							
Classed as healthy	10	2	2	14	71.43	0.79	0.66
Classed as slightly damaged	2	7	0	9	77.78		
Classed as severely damaged	0	0	5	5	100.00		
Sum	12	9	7	28			
Producer's accuracy (%)	83.33	77.78	71.43				
MTVI							
Classed as healthy	8	2	1	11	72.73	0.71	0.56
Classed as slightly damaged	4	7	1	12	58.33		
Classed as severely damaged	0	0	5	5	100.00		
Sum	12	9	7	28			
Producer's accuracy (%)	66.67	77.78	71.43				

Table 6. Confusion matrices and classification accuracies produced by multiple spectral features with the MLC method

Predicted classes	Reference				User's accuracy (%)	Overall accuracy (%)	kappa coefficient
	Healthy	Slightly damaged	Severely damaged	Sum			
Single-date image (13 August)							
Classed as healthy	2	0	1	3	66.67	0.39	0.11
Classed as slightly damaged	9	7	4	20	35.00		
Classed as severely damaged	1	2	2	5	40.00		
Sum	12	9	7	28			
Producer's accuracy (%)	16.67	77.78	28.57				
Two-date images							
Classed as healthy	4	0	1	5	80.00	0.50	0.25
Classed as slightly damaged	8	8	4	20	40.00		
Classed as severely damaged	0	1	2	3	66.67		
Sum	12	9	7	28			
Producer's accuracy (%)	33.33	88.89	28.57				

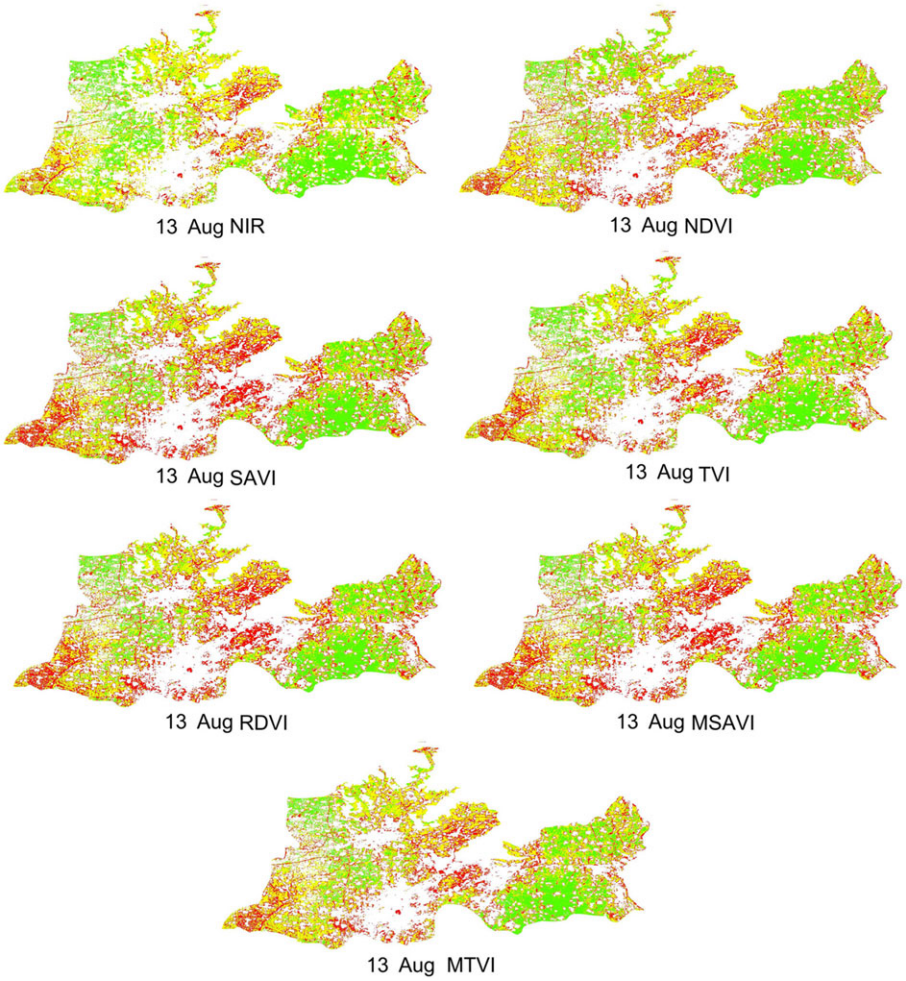

Figure 11. Results of armyworm damage mapping based on multiple spectral features.

mapping accuracy compared with the two-date damage mapping method, with the average overall accuracy (of the tested individual spectral features) decreasing from 0.70 to 0.52 for univariate models. For multivariate models, a similar pattern of mapping accuracy is observed, with overall accuracy decreasing from 0.50 to 0.39.

4 DISCUSSION

In the summer of 2012 in northern China, cool and wet weather coincided with the propagation of armyworm, which thus accounted for a wide expansion of the armyworm population. In addition, the contiguous large maize-planted area also played a key role in promoting the insect infestation by providing an ideal

Table 7. Confusion matrices and classification accuracies produced by individual spectral features from the single-date image (13 August)

	Reference						
Predicted classes	Healthy	Slightly damaged	Severely damaged	Sum	User's accuracy (%)	Overall accuracy (%)	kappa coefficient
NIR							
Classed as healthy	5	2	2	9	55.56	0.46	0.18
Classed as slightly damaged	7	6	3	16	37.50		
Classed as severely damaged	0	1	2	3	66.67		
Sum	12	9	7	28			
Producer's accuracy (%)	41.67	66.67	28.57				
NDVI							
Classed as healthy	9	4	2	15	60.00	0.54	0.26
Classed as slightly damaged	3	4	3	10	40.00		
Classed as severely damaged	0	1	2	3	66.67		
Sum	12	9	7	28			
Producer's accuracy (%)	75.00	44.44	28.57				
SAVI							
Classed as healthy	5	1	2	8	62.50	0.54	0.29
Classed as slightly damaged	7	7	2	16	43.75		
Classed as severely damaged	0	1	3	4	75.00		
Sum	12	9	7	28			
Producer's accuracy (%)	41.67	77.78	42.86				
TVI							
Classed as healthy	5	2	2	9	55.56	0.50	0.24
Classed as slightly damaged	7	6	2	15	40.00		
Classed as severely damaged	0	1	3	4	75.00		
Sum	12	9	7	28			
Producer's accuracy (%)	41.67	66.67	42.86				
RDVI							
Classed as healthy	5	1	2	8	62.50	0.54	0.29
Classed as slightly damaged	7	7	2	16	43.75		
Classed as severely damaged	0	1	3	4	75.00		
Sum	12	9	7	28			
Producer's accuracy (%)	41.67	77.78	42.86				
MSAVI							
Classed as healthy	5	1	2	8	62.50	0.54	0.29
Classed as slightly damaged	7	7	2	16	43.75		
Classed as severely damaged	0	1	3	4	75.00		
Sum	12	9	7	28			
Producer's accuracy (%)	41.67	77.78	42.86				
MTVI							
Classed as healthy	5	1	2	8	62.50	0.50	0.24
Classed as slightly damaged	7	7	3	17	41.18		
Classed as severely damaged	0	1	2	3	66.67		
Sum	12	9	7	28			
Producer's accuracy (%)	41.67	77.78	28.57				

habitat. In damage by armyworm to maize, the insect primarily fed on foliage, which thereby resulted in a significant reduction in leaf area and biomass. By comparison, dehydration and destruction of the pigmentary system by the insects were secondary. Such damage characteristics explain the response patterns of LAI and SPAD values in Fig. 7. Changes in biophysical parameters on account of insect damage serve as a basis of the sensitivity of spectral features. Among the four original band reflectances, the NIR band showed a stronger sensitivity to insect damage than the other three visible bands for both single-date and two-date mapping, which was associated with variation in canopy multi-scattering driven by change in LAI.[9] Most of the VIs exhibiting higher sensitivity to damage apply algebraic procedures based on original bands, which enhance the spectral responses from different aspects. It was also noted that all VIs contained an NIR band, which thereby had the potential to be sensitive to LAI variation and might explain their good performance in mapping the armyworm.

In this study, compared with the maps produced with two-date spectral features, the performance of single-date spectral features suggested that the insect damage was not mapped well enough by single-date remote sensing data (Tables 5 to 7). Compared with two-date mapping results, the significantly larger commission error of single-date mapping implied that, apart from insect

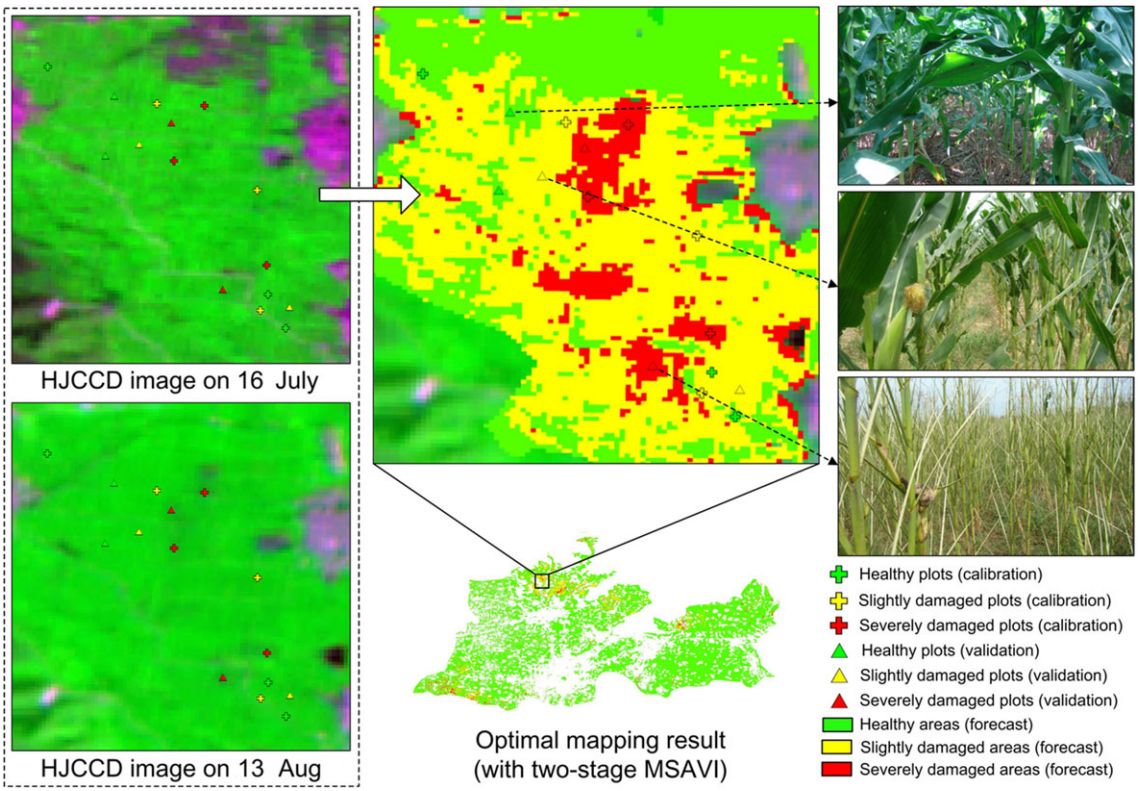

Figure 12. Original images and mapping results of armyworm infestation in a subregion (based on the optimal two-date MSAVI).

damage, there were other factors leading to responses of the same spectral features, which resulted in a dramatic expansion of the 'infested area' (Figs 9 to 11). It is understandable that, within a single-date image scene, the spectral features would not only respond to insect damage but also vary according to phenological differences (e.g. fields in southern parts grew a little earlier than in the remaining areas), cultivar differences and variation in plant vigour between fields.[6] The spectral change between stages before and after the armyworm attack event helps to eliminate field anomalies other than the armyworm infestation, which thereby leads to a sound improvement in accuracy compared with single-date mapping results. Such a pattern confirmed that the mapping protocol based on two-date images as proposed in this study is reasonable and effective for mapping armyworm infestation. Among spectral features, MSAVI produced the highest accuracy. The modified SAVI is able not only to resist the influence of soil background but also to respond to LAI dynamics in a wider range than SAVI.[35,36] Such a trait of the index makes it more suitable for monitoring the damaged fields with LAI varying from very low (almost with only the plant stems left) to high. It was encouraging that the univariate model outperformed multivariate models in mapping the armyworm in this study. We assumed that the mechanism of spectral response to insect destruction was relatively simple and direct, which had a good linearity with a single VI. However, in spite of the multiple variables in multivariate models providing abundant information, the information redundancy issue might cause a reduction in model accuracy.

Apart from insect damage maps of the entire study area, a subset of mapping results produced by optimal two-date MSAVI, as well as original images at both stages, is shown in Fig. 12, which allows a direct visual observation of spectral change and corresponding damage severity. As the image-based estimation of damage severity was highly consistent with our field observations (see Fig. 12 for scenes of the field survey), the effectiveness of the method was confirmed. In contrast to manual interpretation, a semi-automatic delineation method as described in this study helps to eliminate interpreter bias and can thus increase the consistency and reliability of mapping between different areas or dates.[43,44] More importantly, such a remote sensing (RS)-based workflow provides a fast and effective way to extend point observation to an entire region in a spatially continuous manner, which would be a labour-saving mode in crop damage monitoring. For the armyworm outbreak event in the summer of 2012 in Tangshan, our study results provided timely information about the spatial distribution of infestation and damage severity for the Plant Protection Agency of Hebei Province, China. The information has greatly facilitated the agency's strategic planning and decision-making in crop production management.

In this study, although the two-date moderate-resolution HJ-CCD satellite image data showed a sound performance in mapping and determining severity of the armyworm infestation, the accuracy was expected to be higher than 80%, as has been achieved in crop pest mapping study cases with high-resolution airborne or satellite images.[24,45,46] There may be several reasons for the moderate accuracy in the present study. Firstly, a mixed pixel problem is inevitable for a moderate resolution image. In spite of the comprehensive field survey strategy adopted in this study (see Section 2.2), it is still impossible to eliminate completely the influence of the mixed pixel problem. Secondly, the error from coregistration between image scenes (i.e. images acquired on two dates) will also bring uncertainty in subsequent change detection processes. Further, as shown in the confusion matrices (Tables 4 to 6), the slightly damaged samples were significantly underestimated (many of them were misclassified as healthy), which might

be related to the feeding habit of armyworm. Given the fact that the feeding of armyworm results in damage to maize foliage from bottom to top, most leaves on the top of maize remain undamaged for slightly damaged plants. In this case, such plants might have a slight spectral change, thereby lacking a clear spectral signature to be sensed. To solve the problem, it might be helpful to apply multiangular remote sensing observations to reflect the change in middle to lower layers of maize plants.[47] As this study presented an RS-based workflow for mapping insect damage that had already occurred, it would be more important to develop strategies for damage prediction. In spite of methods driven by meteorological data being mainstream for disease/insect prediction, it is believed that the synergy between meteorological data and RS data on damage prediction has a promising future.[48] RS observations have been proven to have great potential in obtaining information about crop biophysical status and habitat characteristics (e.g. vegetation coverage, leaf area index, biomass, soil water content, land surface temperature, etc.) that are not reflected by meteorological observations. Therefore, it is recommended that advantage be taken of the mutual complementary traits of meteorological data and RS data, and that a synergetic scheme be developed for predicting crop disease/insect damage at an early stage.

5 CONCLUSIONS

Monitoring of armyworm at a regional scale is of practical importance, given that the insect tends to develop quickly, but that this development is difficult to forecast precisely. In this study, a method for mapping armyworm damage based on multispectral satellite remote sensing data has been developed and tested, ensuring a systematic census of insect infestation over a large area. Our results suggest that a combination of multispectral moderate-resolution satellite imagery and an optimised thresholding strategy is able to produce a reasonable insect damage map with an overall accuracy of 0.79. Therefore, such a method could provide an economic and efficient alternative to conventional methods, which mainly depend on laborious field investigations.

The potential application of mapping results of armyworm infestation derived from remote sensing data facilitates loss assessment for the agricultural insurance industry by using information on the spatial distribution of insect damage. For example, mapping results can be used for identifying suspected areas that require intensive field surveys, allocating limited supplies (e.g. pesticides, sprayers) and deploying experienced experts to direct prevention operations. In the future, with high-resolution space-borne remote sensing data becoming more available and less expensive, mapping results at a finer scale (e.g. parcel level) are expected further to enhance operational capability. In this domain, more efforts and studies are needed to improve the reliability and robustness of mapping techniques.

ACKNOWLEDGEMENTS

This work was financially supported by the National Natural Science Foundation of China (Project Nos 41301476 and 41271412), the Beijing Natural Science Foundation (Project No. 4132029), and Beijing Nova Programme (No. Z151100000315059), China. The authors are grateful to Mrs Shuhong Cai from Hebei Plant Protection Agency and to Mr Weiguo Li and Mrs Hong Chang from the Beijing Research Centre for Information Technology in Agriculture for their assistance in data collection.

REFERENCES

1 Pimentel D, McLaughlin L, Zepp A, Lakitan B, Kraus T, Kleinman P *et al.*, Environmental and economic effects of reducing pesticide use in agriculture. *Agric Ecosyst Environ* **46**:273–288 (1993).
2 Peshin R and Dhawan AK, *Integrated Pest Management. Vol. 1. Innovation-Development Process*. Springer, Dordrecht, The Netherlands (2009).
3 Girdžiūtė L, Risks in agriculture and opportunities of their integrated evaluation. *Proc-Soc Behav Sci* **62**:783–790 (2012).
4 Moran MS, Inoue Y and Barnes EM, Opportunities and limitations for image-based remote sensing in precision crop management. *Remote Sens Environ* **61**:319–346 (1997).
5 Seelan SK, Laguette S, Casady GM and Seielstad GA, Remote sensing applications for precision agriculture: a learning community approach. *Remote Sens Environ* **88**:157–169 (2003).
6 West JS, Oberti R and Moshou D, The potential of optical canopy measurement for targeted control of field crop diseases. *Annu Rev Phytopathol* **41**:593–614 (2003).
7 Hahn F, Actual pathogen detection: sensors and algorithms – a review. *Algorithms* **2**:301–338 (2009).
8 Sankaran S, Mishra A, Ehsani R and Davis C, A review of advanced techniques for detecting plant diseases. *Comput Electron Agric* **72**:1–13 (2010).
9 Weng QH, Hyperspectral remote sensing of vegetation bioparameters, in *Advances in Environmental Remote Sensing*, ed. by Pu RL and Gong P. CRC Press, Boca Raton, FL, Ch. 5 (2011).
10 Liu LY, Huang WJ and Zhang B, Estimating winter wheat plant water content using red edge parameters. *Int J Remote Sens* **25**:3331–3342 (2004).
11 Chen PF, Haboudane D, Tremblay N, Wang JH, Vigneault P and Li BG, New spectral indicator assessing the efficiency of crop nitrogen treatment in corn and wheat. *Remote Sens Environ* **114**:1987–1997 (2010).
12 Moshou D, Wahlen S, McCartney A and Ramon H, Simultaneous identification of plant stresses and diseases in arable crops using proximal optical sensing and self-organising maps. *Precis Agric* **7**:149–164 (2006).
13 Devandas R, Lamb DW, Simpfendorfer S and Backhouse D, Evaluating ten spectral vegetation indices for identifying rust infection in individual wheat leaves. *Precis Agric* **10**:459–470 (2009).
14 Zhang JC, Pu RL, Wang JH, Huang WJ, Yuan L and Luo JH, Detecting powdery mildew of winter wheat using leaf level hyperspectral measurements. *Comput Electron Agric* **85**:13–23 (2012).
15 Luo JH, Huang WJ, Zhao JL, Zhang JC, Zhao CJ and Ma RH, Detecting aphid density of winter wheat leaf using hyperspectral measurements. *IEEE JSTARS* **6**:690–698 (2013).
16 Fitzgerald GJ, Maas SJ and Detar WR, Spider mite detection and canopy component mapping in cotton using hyperspectral imagery and spectral mixture analysis. *Precis Agric* **5**:275–289 (2004).
17 Yang CM and Chen RK, Changes in spectral characteristics of rice canopy infested with brown planthopper and leaffolder. *Crop Sci* **47**:329–335 (2007).
18 Wang X, Zhang M, Zhu J and Geng S, Spectral prediction of *Phytophthora infestans* infection on tomatoes using artificial neural network (ANN). *Int J Remote Sens* **29**:1693–1706 (2008).
19 Yang CM, Assessment of the severity of bacterial leaf blight in rice using canopy hyperspectral reflectance. *Precis Agric* **11**:61–81 (2010).
20 Xu HR and Fu XP, Near-infrared spectroscopy in detecting leaf miner damage on tomato leaf. *Biosyst Eng* **96**:447–454 (2007).
21 Naidu RA, Perry EM, Pierce FJ and Mekuria T, The potential of spectral reflectance technique for the detection of Grapevine leafroll-associated virus-3 in two red-berried wine grape cultivars. *Comput Electron Agric* **66**:38–45 (2009).
22 Huang W, Niu Z and Liu L, Identification of yellow rust in wheat using *in-situ* spectral reflectance measurements and airborne hyperspectral imaging. *Precis Agric* **8**:187–197 (2007).
23 Qin ZH and Zhang MH, Detection of rice sheath blight for in-season disease management using multispectral remote sensing. *Int J Appl Earth Obs* **7**:115–128 (2005).
24 Franke J and Menz G, Multi-temporal wheat disease detection by multi-spectral remote sensing. *Precis Agric* **8**:161–172 (2007).
25 Chen X, Qiao H and Xu Y, Detecting infestation of take-all disease in wheat using Landsat Thematic Mapper imagery. *Int J Remote Sens* **28**:5183–5189 (2007).

26 Stohlgren TJ, Barnett DT and Crosier CS, *The North American Weed Management Association Standards*. [Online]. NAWMA (2005). Available: http://www.nawma.org/documents/Mapping%20Standards/BEYOND%20NAWMA%20STANDARDS.pdf [20 June 2012].
27 Tang H, Zhang B and Tian Y, Comparison of photosynthetic characteristics of three-ear-leaf hybrid maize. *J Maize Sci* **2**:23 (2009).
28 Yang FT, Gu XH, Li G, Cao QJ, Jiang XL and Wang JH, Monitoring spatial distribution of armyworm disaster on maize with multi-temporal HJ-CCD images. *Trans CSAE* **14**:21 (2013).
29 Silva P, Braga JD and Oliveira OF, Nitrogen doses and weed control via intercropping with gliricidia for corn production. *Planta Daninha* **28**:531–539 (2010).
30 Chen YG, Ni XZ and Buntin GD, Physiological, nutritional, and biochemical bases of corn resistance to foliage-feeding fall armyworm. *J Chem Ecol* **35**:297–306 (2009).
31 Liang SL, Fang HL and Chen MZ, Atmospheric correction of Landsat ETM+ land surface imagery – Part 1: Methods. *IEEE Trans Geosci Remote Sens* **39**:2490–2498 (2001).
32 Zhang JC, Pu RL, Yuan L, Wang JH, Huang WJ and Yang GJ, Monitoring powdery mildew of winter wheat by using moderate resolution multi-temporal satellite imagery. *PLoS ONE* **9**:e93107 (2014).
33 Rouse JW, Haas RH, Schell JA and Deering DW, *Monitoring vegetation systems in the Great Plains with ERTS, in NASA SP-351*. NASA, Washington, DC, 309 pp. (1974).
34 Roujean J and Breon F, Estimating PAR absorbed by vegetation from bidirectional reflectance measurements. *Remote Sens Environ* **51**:375–384 (1995).
35 Broge NH and Leblanc E, Comparing prediction power and stability of broadband and hyperspectral vegetation indices for estimation of green leaf area index and canopy chlorophyll density. *Remote Sens Environ* **76**:156–172 (2000).
36 Haboudane D, Pattey E and Strachan IB, Hyperspectral vegetation indices and novel algorithms for predicting green LAI of crop canopies: modeling and validation in the context of precision agriculture. *Remote Sens Environ* **90**:337–352 (2004).
37 Huete AR, A soil-adjusted vegetation index (SAVI). *Remote Sens Environ* **25**:295–309 (1988).
38 Qi J, Chehbouni A, Huete AR, Kerr YH and Sorooshian S, A modified soil adjusted vegetation index. *Remote Sens Environ* **48**:119–126 (1994).
39 Lu D, Mausel P, Brondizio E and Moran E, Change detection techniques. *Int J Remote Sens* **25**:2365–2401 (2004).
40 Pu R and Landry S, A comparative analysis of high resolution ikonos and worldview-2 imagery for mapping urban tree species. *Remote Sens Environ* **124**:516–533 (2012).
41 Zhang JC, Pu LR, Yuan L, Wang JH, Huang WJ and Yang GJ, Monitoring powdery mildew of winter wheat by using moderate resolution multi-temporal satellite imagery. *PLoS ONE* **9**:e93107 (2014).
42 Congalton R and Mead RA, A quantitative method to test for consistency and correctness in photointerpretation. *PE&RS* **49**:69–74 (1983).
43 White JC, Wulder MA, Brooks D, Reich R and Wheate RD, Mapping mountain pine beetle infestation with high spatial resolution satellite imagery. *For Chron* **80**:743–745 (2004).
44 Coops N, Culvenor D, Preston R and Catling P, Procedures for predicting habitat and structural attributes in eucalypt forests using high spatial resolution remotely sensed imagery. *Aust For* **61**:244–252 (1998).
45 Hicke JA and Logan J, Mapping whitebark pine mortality caused by a mountain pine beetle outbreak with high spatial resolution satellite imagery. *Int J Remote Sens* **30**:4427–4441 (2009).
46 Oumar Z and Mutanga O, Using WorldView-2 bands and indices to predict bronze bug (*Thaumastocoris peregrinus*) damage in plantation forests. *Int J Remote Sens* **34**:2236–2249 (2013).
47 Dorigo WA, Improving the robustness of cotton status characterisation by radiative transfer model inversion of multi-angular CHRIS/PROBA data. *IEEE JSTARS* **5**:18–29 (2012).
48 Zhang JC, Pu RL, Yuan L, Huang WJ, Nie CW and Yang GJ, Integrating remotely sensed and meteorological observations to forecast wheat powdery mildew at a regional scale. *IEEE JSTARS* **7**:4328–4339 (2014).